

Vertex analysis of the 2015 Engineering Run

Matthew Solt

Stanford University, Stanford, CA

Mathew Graham

SLAC National Accelerator Laboratory, Menlo Park, CA

Holly Szumila-Vance

Thomas Jefferson National Laboratory, Newport News, VA

Sho Uemura

Los Alamos National Laboratory, Los Alamos, NM

Abstract

The Heavy Photon Search experiment Engineering Run took data during the spring of 2015 at Jefferson lab with a 1.056 GeV electron beam at 50 nA incident on a 4 μm thick tungsten target. This note describes the analysis developed for searching for heavy photons with a detached vertex with the SVT at the nominal 0.5 mm SVT position and uses tracks that pass through the first layer of the tracker. All cuts and studies were done on 100% of the data so as to study backgrounds on the full data set. The purpose of this note is to establish the procedure and cuts, establish limits, and lay the framework for future vertex searches.

1 Introduction to Vertex Search

The search for heavy photons with displaced vertices is centered on the premise that the experimental vertex resolution is roughly Gaussian ($N \propto e^{-z^2/\sigma^2}$) and that heavy photons have a measurable lifetime with an exponential decay length ($N_{A'} \propto e^{-z/\gamma c\tau}$). Therefore, beyond a certain distance z from the target, there should be almost no background but still some A' signal. The goal of this analysis is to search for the heavy photon signal in a region of little to no background. We choose two-cluster events with an energy sum greater than 80% of the beam energy having tracks that match to ECal clusters. We reconstruct the vertex position between the pairs of tracks at the point of closest approach and measure the invariant mass of the e^+e^- pair from the measured three-momenta. We select an unbiased sample of events with low background by choosing a downstream position z_{Cut} at which we can reject backgrounds and search for signal events.

1.1. General event selection

The event selection for the vertex analysis was initially optimized using a blinded data analysis such that the cuts were tuned on 10% of the data and then was developed on the full data set. While the search should be performed on a data set using a blind analysis, it was realized early on that we had more backgrounds than we had originally anticipated, and our reach was significantly reduced due to not accounting for acceptance-related effects. The decision to unblind the data was made after significant effort to minimize backgrounds.

The events relevant to the vertex analysis were selected using the Pairs 1 HPS trigger. This loose trigger selects events that have one cluster each in the top and bottom halves of the ECal. The measured sum of the energy of the two reconstructed particles is chosen to be greater than 80% of the beam energy to keep possible A' events and reject Bethe-Heitler background. Tracks are reconstructed using various hypotheses, and a Generalized Broken Lines (GBL) track re-fit is performed using a minimum of five hits in a track. The closest approach of an e^+e^- track pair is used to construct the vertex using an unconstrained vertex fit. The vertex χ^2 quality of a beam spot constrained fit to the e^+e^- pair was used to determine how well the momentum of the pair projects back to the beam spot position at the target. We additionally use the re-fit momenta of the two particles at the unconstrained vertex to reconstruct the projected vertex position at the target.

The SVT reconstructed tracks are projected to the ECal and matched to clusters based on position as a function of momentum. The match quality is measured in standard deviations, $n\sigma$, of the position difference for a given momentum. Due to the ECal having better timing resolution than the SVT, the time difference between two clusters is used to eliminate accidental coincidences and to study background contributions from accidentals. There are a few cuts that originate specifically from studies of high z background events and physics processes. These include cuts on the e^+e^- momentum asymmetry, the number of hits shared between reconstructed positron tracks, and most significantly, a 3σ cut on the vertex projection to the beam spot position at the target.

1.1.1 Vertex constraints

The vertex search uses the unconstrained vertex fit to determine the z vertex position of the e^+e^- pair. The unconstrained fit uses only the distance of closest approach between the two tracks. We used the quality of the beam spot constrained fit, which considers both the point of closest approach between the two tracks and the momentum projection back to the beam spot position

at the target, only as a data quality cut. For genuine A' displaced vertices, the z vertex position is relatively unchanged when using a beam spot constrained versus an unconstrained vertex fit. An incorrect beam spot position can systematically pull a measured vertex position. Background events from prompt vertices that are pushed to large z through measurement error or scatters can be arbitrarily biased in the z vertex position by using the beam spot constrained fit. For these reasons, the unconstrained fit is used to determine z .

1.2. Datasets

We took 1.7 days (1166 nb^{-1}) of data with a 1.056 GeV beam with the SVT at the nominal position where Layer 1 is at ± 0.5 mm from the beam. We took an additional 0.47 days (362.7 nb^{-1}), prior to moving the SVT to the nominal position, with the SVT Layer 1 at ± 1.5 mm from the beam. A large portion of the data taken with the first layer of the SVT at ± 1.5 mm was unusable due to an incorrect timing latency in the SVT DAQ and is excluded from this analysis. To extract the full reach of the data, one should consider all of the data from mutually exclusive data sets where both the e^+e^- have tracks with hits in the first SVT layer, one particle has a track in the first layer and both tracks have their first hits in the second layer. The over all statistics of each data set using the pass 8 reconstruction for the 0.5 mm data are shown in Table 1. Events were excluded where the reconstructed track passed through the active region of the Layer 1 sensor and had no hit.

Table 1: *Vertexing Data sets*

Data sets	First hit of track	SVT position	events
L1L1	Both tracks layer 1	0.5 mm	13,329,700
L1L2	One track layer 1	0.5 mm	152,406
L2L2	Both tracks layer 2	0.5 mm	1,446

The track reconstruction will find tracks with hits in any 5 out of the 6 layers. This means that tracks can be reconstructed without layer 1 hits (as long as they have hits in all other layers). Tracks without layer 1 hits have degraded mass and vertex resolution. Furthermore, the tails of the vertex distribution extend to larger values of z . For these reasons, it is not possible to use tracks with and without layer 1 hits as part of the same data set. For simplicity, this analysis is limited to pairs with layer 1 hits on both tracks. The background from wide-angle bremsstrahlung conversions is also significantly reduced by this cut. In order to create charged tracks, the bremsstrahlung photon must convert in the target, either layer 1 sensor, or early enough in the upstream layer 2 sensor to make a hit there. But in order to create charged tracks with layer 1 hits, the photon must convert in the target or the upstream layer 1 sensor. The silicon sensors ($0.35\% X_0$) are significantly thicker than the portion of the target traversed by the average photon (half of $0.125\% X_0$), so requiring that the track have a layer 1 hit cuts this background by roughly a factor of three. This note will focus on the backgrounds and data in the L1L1 data set only.

This data set corresponds to the pass 8 reconstruction. This was the first reconstruction pass where vertices were properly re-fit and track re-fit parameters were not required to correspond to the target reference point (allowing for downstream vertex reconstruction). This fix was essential for eliminating a z -dependence of the reconstructed mass. The geometry that corresponds to this pass assumes the target position to be located at the nominal 0 mm downstream.

2 Displaced Heavy Photon Signal

Heavy photon production, for both prompt and displaced vertices, is related to the radiative trident cross section. In looking for heavy photons with displaced vertices, the vertex distribution is characterized with the reconstructed invariant mass of the e^+e^- pair, and events of interest are identified as originating far beyond the tails of the prompt trident backgrounds.

We must select a downstream region when searching for a displaced heavy photon having virtually no background. Therefore, we choose a $zCut$ which is a downstream z vertex position beyond which there should be fewer than 0.5 background events per mass bin. We arbitrarily choose our maximum z value, $zMax$, to be at the first layer, although this is actually suppressed by the geometry acceptance when we choose both tracks to have hits in layer 1. The $zCut$ varies as a function of mass and, ideally, can be selected to minimize backgrounds whilst maximizing A' reach efficiency. If an A' exists, then the number of events we can expect to reconstruct is

$$S_{bin,zCut} = \left(\frac{N_{rad}}{N_{tot}} \right) N_{bin} \left(\frac{3\pi\epsilon^2}{2N_{eff}\alpha} \right) \left(\frac{m_{A'}}{\delta m_{A'}} \right) \epsilon_{bin} \int_{zCut}^{zMax} \frac{e^{-z/tgt-z/\gamma c\tau}}{\gamma c\tau} \epsilon_{vtx}(z, m_{A'}) dz \quad (1)$$

where the heavy photon production at the target per mass bin is described by the first four terms. N_{rad}/N_{tot} is the fraction of radiative events (see Figure 1) contained in the sample and is derived from Monte Carlo. N_{bin} is the number of measured e^+e^- pairs at a given mass. The third and fourth terms are explained in Equation (2). ϵ_{bin} is the fraction of the number of signal events contained within our selected mass bin window (we choose a mass window of $\pm 1.9\sigma_m$ corresponding to an ϵ_{bin} of 0.94 as optimized from data). The integral calculates the expected number of heavy photons we would reconstruct in the decay region from $zCut$ to $zMax$, where z/tgt is the target location. ϵ_{vtx} represents the efficiency of detecting e^+e^- pairs from an A' of mass $m_{A'}$ that decayed at position z from the target and is inclusive of the efficiencies of all other cuts used in the analysis. Based on Poisson statistics, the 90% confidence limit for a null result requires us to have an expected number of A' events to be greater than 2.3.

2.1. Radiative fraction

Background events can be produced by QED trident processes and by wide-angle bremsstrahlung (WAB). The trident processes can be separated into ‘‘radiative’’ and ‘‘Bethe-Heitler’’ diagrams. The heavy photon cross section is related to the radiative trident cross section. The A' production for a mass bin is

$$\frac{d\sigma(A' \rightarrow e + e-)}{d\sigma(\gamma^* \rightarrow e + e-)} = \left(\frac{3\pi\epsilon^2}{2N_{eff}\alpha} \right) \left(\frac{m_{A'}}{\delta m_{A'}} \right) \quad (2)$$

where N_{eff} , the number of available decay states, is one for the HPS experiment which explores a mass range in which the heavy photon can only decay to one Standard Model final state (e^+e^-). ϵ^2 is the coupling factor between the heavy photon and the Standard Model, and α is the fine structure constant. $\frac{m_{A'}}{\delta m_{A'}}$ is the center of the mass bin divided by the bin width.

The fraction of radiative trident events among all trident events in the HPS search region is the radiative fraction. Using MadGraph5 Monte Carlo to model the tridents and radiatives and the MadGraph4 Monte Carlo to model the wide angle bremsstrahlung (WAB) background, we found the radiative fraction to be approximately 9.5% for all masses (see Figure 1). This fraction is defined as the ratio of radiative events to all events (tritrig+WAB in Figure 1). As shown in Figure 1, the radiative fraction relevant to the vertex analysis is approximately 9.5% for all masses.

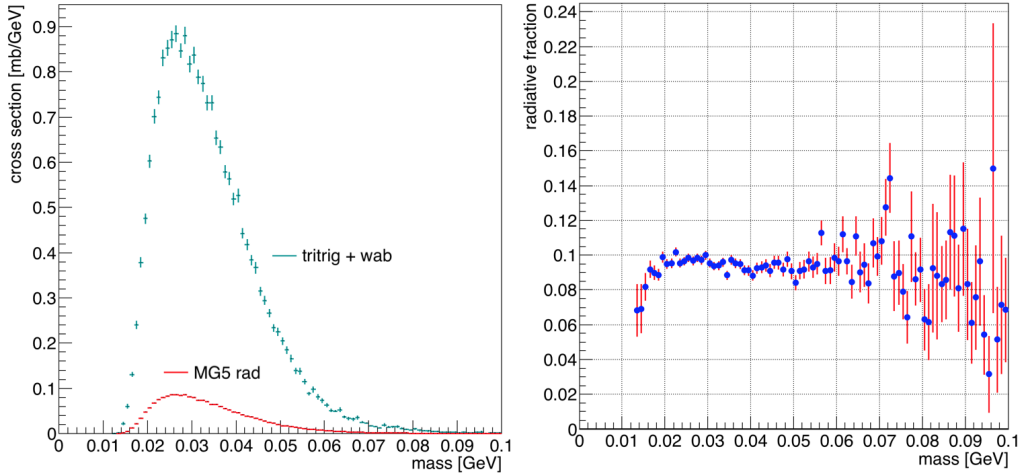


Figure 1: The radiative fraction is the fraction of radiative events to all measured events. The plot on the left shows the background containing all trident diagrams and wide angle bremsstrahlung, inclusively, in green and the radiatives in red. The ratio between these two curves is shown on the right with a roughly constant radiative fraction of 9.5%.

2.2. Reconstructed z vertex

The reconstructed z vertex ϵ_{vtx} is defined as the product of the trigger, track reconstruction, vertex reconstruction, and cut efficiencies as well as the acceptance. It is found by taking the A' Monte Carlo after full detector simulation and analysis cuts and dividing by the truth A' Monte Carlo with $c\tau = 10$ mm. This is done as a function of truth z decay position. The $c\tau$ value is chosen to populate enough A' statistics in the region of interest and has no effect on the efficiency. Sample efficiencies are shown in Figure 2 for a variety of A' masses. The efficiency curves fall rapidly (quicker than an exponential tail) due to acceptance effects for longer lived A' s and the requirement of layer 1 SVT hits.

For the reach estimates and limit setting, the normalized efficiency curves are used since the expected A' rate is normalized directly from data. This includes the mass dependent target position see in Fig. 8 from which the A' yield was calculated from in the final reach and limit estimates calculated in Section 4. In order to grab mass and z values inbetween the values on the histograms, a basic bilinear interpolation is used. The values from this interpolation is used for the $\epsilon_{vtx}(z, m_{A'})$ value in Equation (1).

2.3. Mass resolution

The mass resolution in pass 8 is independent of the reconstructed z vertex position. This observation is a great achievement for the pass 8 reconstruction as the track parameters are now adjusted for the vertex position. The general vertex fitting procedure is discussed in [P. Billoir, 1992]. To verify that the mass resolution is stable with decay vertex position, A' Monte Carlo was used to first check the reconstructed vertex and then to parameterize the mass resolution. The reconstructed mass residual for a Monte Carlo A' at a representative mass is shown in Fig. 3. The mass resolution is initially determined from A' Monte Carlo and then scaled according to the difference between the Monte Carlo Møller and data mass resolution. By generating heavy photons at discrete masses, applying the cuts proposed in data, and fitting the A' mass peak residual with

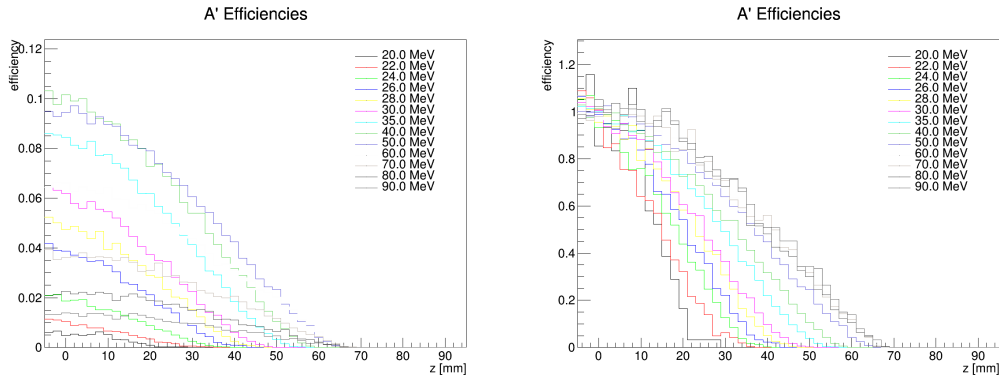


Figure 2: A' efficiencies as a function of truth decay z for various masses. A' s were simulated using $c\tau = 10$ mm in order to generate decays to the first layer of the SVT, but the efficiency is independent of this value. Left: The efficiencies of the A' versus their decay position defined as the ratio of reconstructed over generated. Right: The same efficiencies shown on the left but all are normalized to unity at the target position. Larger masses have larger opening angles in the lab frame and, therefore, have higher probabilities to being detected in layer 1 of the SVT. Pairs with smaller opening angles that decay downstream may not be observed due to geometric acceptance.

respect to the generated mass peak, the mass resolution is obtained as a function of mass. A fit to the generated 40 MeV heavy photon in Monte Carlo is shown in Figure 4. Simulations of the Møller mass can be used to study systematic offsets between the measured mass resolution in data and the mass resolution found in Monte Carlo. Using Møller Monte Carlo, the Møller mass can be seen on the left in Figure 5. The Møller mass resolution from Monte Carlo is about 17% larger than the Møller mass resolution found in data. The heavy photon mass resolution found in Monte Carlo was increased by 17% in order to appropriately scale the bin widths when slicing and fitting the vertex distribution by mass. The Møller peak from data is shown on the right in Figure 5.

The mass resolution is shown in Figure 6 as a function of mass. After applying the 17% scaling to the mass resolution from A' Monte Carlo, we obtain the mass resolution

$$\sigma_m = 0.02436m + 0.0007 \text{ GeV} \quad (3)$$

used in the vertex analysis to find the z vertex cut.

2.4. Determining $zCut$

In order to look for heavy photons with displaced vertices, one must fully characterize the distribution of events and trident production at the target so that a value of $zCut$ can be selected. Beyond $zCut$, we expect to remove all prompt trident backgrounds. While this search is ideally suited to search with no backgrounds, we must further account for the few events that lie beyond $zCut$ due to scattering in the silicon. $zCut$ varies with the reconstructed mass. To find the value of $zCut$ for each mass hypothesis, we slice the distribution of the reconstructed vertex position versus reconstructed mass in bins of mass. We fit the core of the vertex distribution with a Gaussian and fit the downstream tail of the distribution with an exponential. The fit for the full vertex

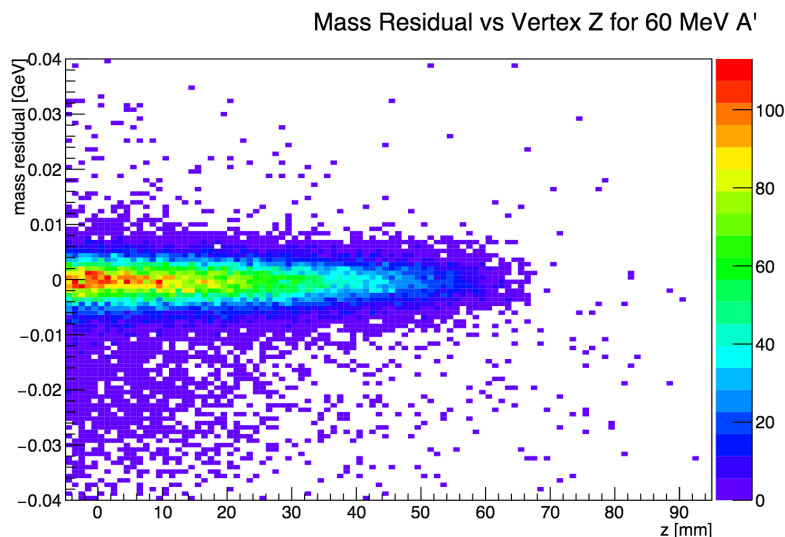


Figure 3: The mass residual of a reconstructed 60 MeV A' is shown as a function of vertex position in z . The resolution is stable, as anticipated.

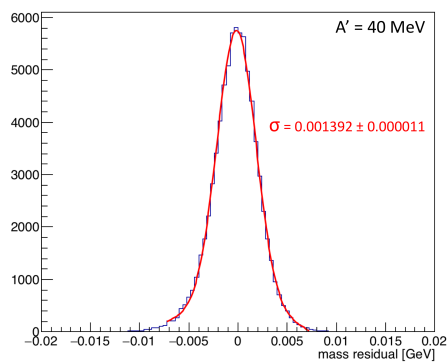


Figure 4: The residual of a reconstructed 40 MeV A' mass is shown with a Gaussian fit.

distribution in a given mass bin is:

$$F\left(\frac{z - z_{\text{mean}}}{\sigma_z} < b\right) = A e^{-\frac{(z - z_{\text{mean}})^2}{2\sigma_z^2}}$$

$$F\left(\frac{z - z_{\text{mean}}}{\sigma_z} \geq b\right) = e^{-\frac{b^2}{2} - b \frac{z - z_{\text{mean}}}{\sigma_z}}$$
(4)

where b defines the distance from the core of the Gaussian in $n\sigma_z$ at which the downstream tail deviates from the Gaussian description and follows an exponential tail. The fit to a slice for a particular mass hypothesis is shown in Fig. 7. The exponential tail is relatively unaffected by single events from large scatters at far displaced z . We selected the z_{Cut} by integrating the tail and finding the z position beyond which there would extrapolate to be 0.5 events in the background. We selected this value as an assumption that we could therefore expect a negligible background

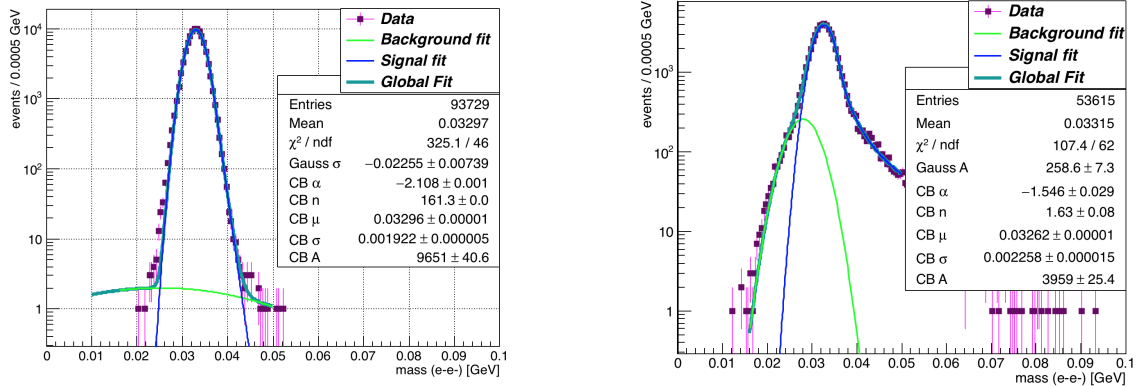


Figure 5: The Møller mass peak from Monte Carlo with a Crystal Ball fit is shown on the left with the background fit using a Gaussian. The same fit models are then applied to the Møller mass in data, shown on the right.

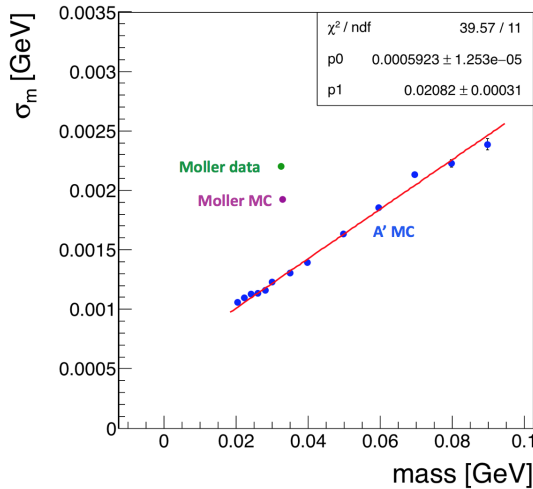


Figure 6: [

Mass resolution compared between Monte Carlo and data] The mass resolution for Møller data (green), Møller Monte Carlo (magenta), and A' Monte Carlo (blue) is shown. The red line $\sigma_m = 0.02082m + 0.0006$ GeV is fit to the A' mass resolution. The difference between the Monte Carlo and data Møller mass resolutions is approximately 17%. This scaling should be applied to the linear fit of the A' mass resolution from Monte Carlo in order to account for the difference in resolution.

for searching for far displaced heavy photon vertices. The selection of $zCut$ is pushed farther downstream logarithmically with increasing statistics in the mass bin and should be, ideally, as small as possible to optimize our reach for an A' signal. On the right in Fig. 7, we see clearly that the downstream fall off of the A' distribution differs significantly with out fit to the prompt scatters and decays at the target. In order to obtain measure the maximum A' signal possible in this experiment, most of our specific event selection cuts focus on eliminating scattering background events that occupy the tails downstream of the target position. The $zCut$ is shown in Fig. 8 where the reconstructed z vertex position for all events in the L1L1 2015 data set are shown versus their reconstructed mass.

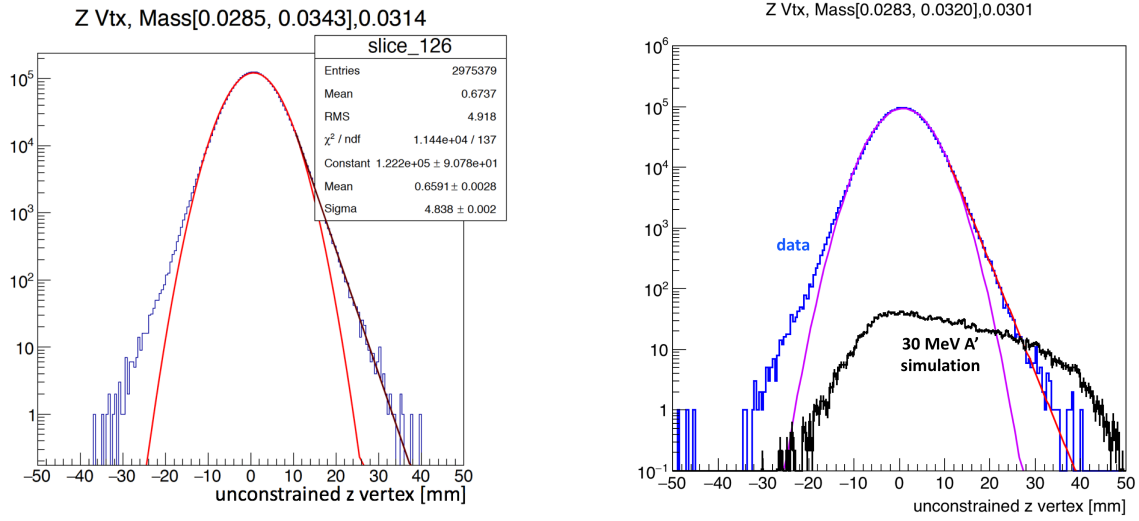


Figure 7: Left: The vertex distribution for a mass hypothesis of 31 MeV from the L1L1 data set is shown. The fit functions are described by Equation (4) where the core of the distribution is fit with a Gaussian and the downstream tail is fit with an exponential. The exponential fit parameters are not shown in the statistics box. Right: The vertex distribution for a mass slice from data (blue) with Gaussian core fit (magenta) and downstream exponential tail fit (red) overlaid with an simulated A' Monte Carlo at the same mass (black). The tail distribution falls off more slowly compared to the distribution of events and scattering tails from the target. For this particular mass slice, the z Cut was found to be at 37.6 mm.

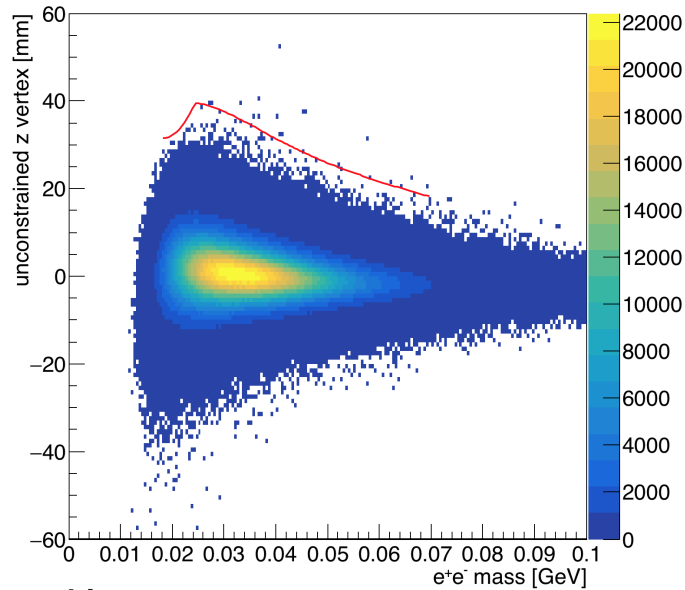


Figure 8: The reconstructed z vertex is shown versus the reconstructed mass of the e^+e^- pair for all events in the 2015 L1L1 data set. The z Cut is obtained by slicing this distribution by mass hypothesis (window size of $\pm 1.9\sigma_m$) and fitting each z vertex distribution with Eq. (4). The z Cut shown in red is the point beyond which we would expect 0.5 background events based on the fit to the tail.

3 Event selection

The event selection is optimized for choosing well-reconstructed events (good tracks and vertex reconstruction) and tries to eliminate events which could arise from scatters that could produce downstream reconstructed vertices. From A' simulation, we implement cuts that improve our selection of events that have favorable kinematics for selecting heavy photons. We make some initial cuts to the data before our analysis that include checking that the SVT bias voltage was on (SVT at the desired position setting) and that the event was a pairs1-type trigger (this is a loose two cluster trigger). We further require that the pairs that triggered have one cluster in the top and one in the bottom halves of the calorimeter.

After this very general event selection, we apply the radiative cut where we consider events having a sum of e^+e^- momenta greater than 80% of the beam energy. For this particular analysis, we further require that both tracks belonging to the vertexed pair have associated hits in layers 1 and 2 of the SVT. Previously, the requirement of Layer 2 was not used, but as the rates are highest in Layer 1 of the SVT, the extrapolation from Layer 3 to Layer 1 is critical in order to correctly measure the vertex of the track. Additionally, the inefficiency in measuring a hit in Layer 2 is approximately 2% (and is different for electrons and positrons). The layer 1 requirement has a significant effect on the reconstruction efficiency for long-lived, low-mass heavy photons. As seen from the target, all layers of the SVT have their inner edges at ± 15 mrad vertical angle from the beam plane. As seen by a heavy photon decaying downstream of the target, layer 1 is at a significantly larger vertical angle than the others, and so the minimum $m_{A'}$ needed to hit layer 1 is larger. This layer requirement implies that the maximum z for detecting a heavy photon of given $m_{A'}$ is smaller if layer 1 is required. We note that to obtain full reach, further work would be required to extract events that do not have a hit in layer 1. Unfortunately, these events have extremely high backgrounds associated with beam interactions in the dead material of the SVT and have therefore been excluded from this analysis.

All cuts here assume that the radiative, trigger, and layer cuts mentioned above have already been applied. The cuts used on the L1L1 0.5 mm data set are shown in Table 2.

Table 2: Cuts applied to the L1L1 data set.

Cut type	Cut	Cut Value	%cut	%cut core	%cut tails
track	Fit quality	track $\chi^2/dof < 6$	24	–	–
track	Max track momentum	$P_{trk} < 75\%E_{beam}$	11	9	20
track	Isolation		4	1	14
track	kinks in L1 and L2	9	7	16	
vertex	beamspot constraint	$bsc\chi^2 < 10$	28	22	57
vertex	beamspot - unconstrained	$bsc\chi^2 - unc\chi^2 < 5$	15	15	15
vertex	maximum P_{sum}	$< 115\%E_{beam}$	0.5	0.5	0.8
vertex	vertex projects to target	elliptical $3\sigma_{x,y}$	2	1	16
ecal	Ecal SVT matching	$\chi^2 < 10$	5	4	10
ecal	track Ecal timing	$< 4ns$	4	4	5
ecal	2 cluster time diff	$< 2ns$	6	6	9
physics	momentum asymmetry	< 0.5	3	3	5
event	max shared hits in e^+ track	< 5 shared hits	9	9	10

In Table 2, the ‘‘Cut type’’ is a summary of what the cut is intended to have the most significant effect on. The ‘‘Cut’’ describes the cut used, and the corresponding value is shown in the next

column, “Cut Value”. The “% cut” column shows the percentage of the events removed from the entire data set by applying this cut. The “% cut core” column shows the percentage of events removed from the Gaussian core of the vertex distribution. The “% cut tails” column shows the percentage of events removed from the downstream tails of the vertex distribution. Our cuts aim to remove background events in the downstream vertex tails that are the result of scattering backgrounds not from A' decay.

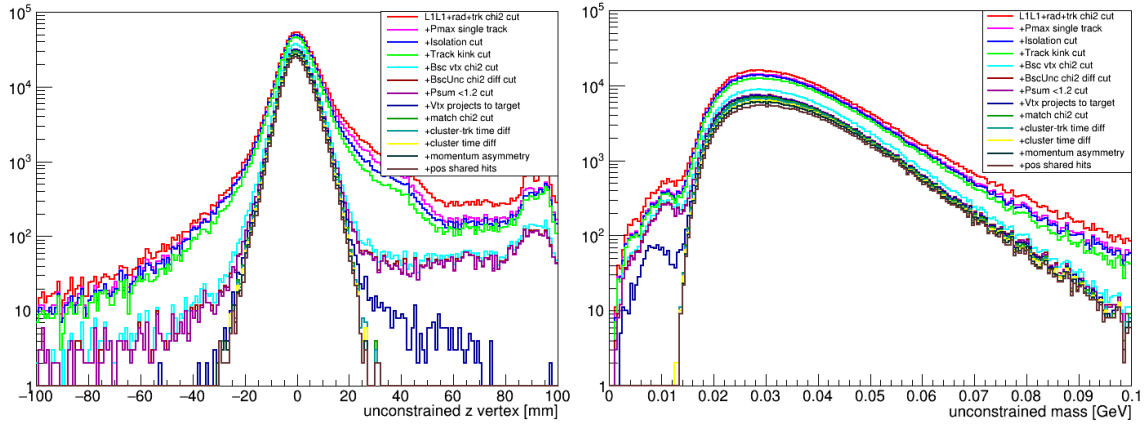


Figure 9: Cut effects on the z vertex distribution for all masses in the L1L1 0.5 mm dataset is shown on the left. The ratio of the z vertex distribution in the final event selection to those events in the initial event selection in the L1L1 0.5 mm dataset is shown on the right.

The effects of the cuts is shown in Fig. 9 in the cumulative order in which the cuts are applied. The left plot shows the effects on the z vertex distribution while the effects on the mass distribution are shown on the right. The initial track fit χ^2 from the Generalized Broken Lines (GBL) fit of the track removes a lot of background and begins to really shape the vertex distribution. This cut value uses the track fit χ^2/dof and is shown in Fig. 10 where all other cuts except for the track quality cut have been applied. After choosing tracks based on their fit qualities, we remove

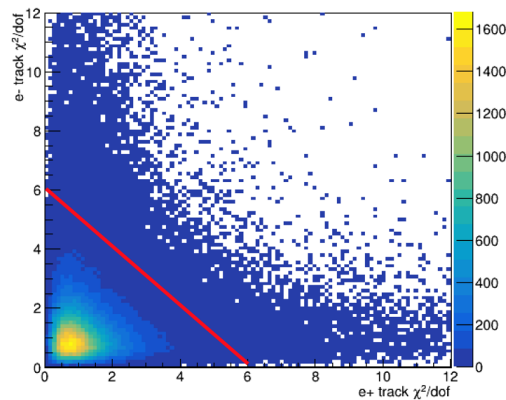


Figure 10: The track quality cut is a cut based on the fit quality of each track for the L1L1 data selection, all tracks have hits in at least 5 of the 6 SVT layers. Shown here is the distribution and cut when all other cuts have been applied.

electron tracks that have greater than 75% of the beam energy. This cut is made to ensure that we

are not choosing elastically-scattered (beam energy) electrons and corresponds also to the general maximum value we can expect for an electron track in trident events (as measured from Monte Carlo). We also include a cut on the maximum momentum of the e^+e^- pair which aims to reduce vertexed pairs that may have come from separate events. This cut removes very few events but is still necessary to ensure that we are not including events that are not correlated.

An isolation cut is also applied to each track to reduce mis-hits in the track, particularly in layer 1, where tracks can be pulled significantly (and thus affect the reconstructed vertex position in z) if the wrong hit is used in the track fit. The isolation value for the electron and the positron in the L1L1 data set is the distance to the next closest hit away from the beam line in Layer 1 relative to the electron and positron hit used in the track. This cut compares the isolation value (parameter δ) to the track projected value in y at the target position (also known as the track z_0 parameter). If the projected isolation to the target is larger than the z_0 parameter at the target, then we assume that the better hit was already chosen for the track. A picture of the variables used in this cut is shown in Figure 11 and described numerically in Equation (5).

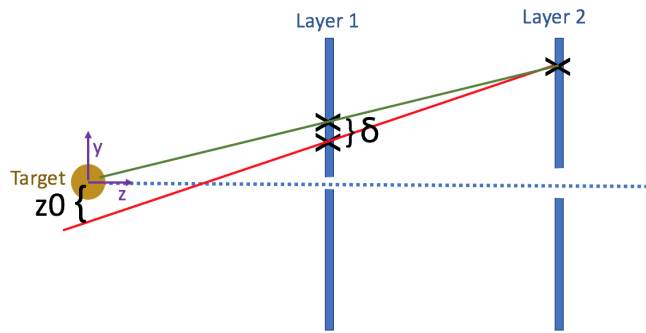


Figure 11: The distance between the closest hit away from the beam plane in Layer 1 is compared to its projection at the target, the track impact parameter z_0 .

$$2\delta + z_0 \times \text{sign}(P_y) > 0 \quad (5)$$

The factor of 2 in Eq. 5 comes because Layer 2 is twice the distance from the target as Layer 1. The z_0 parameter is opposite in sign as compared to the y -component of the track momentum because we only consider downstream vertices. This cut is also a contributing factor to the asymmetrical shape of the overall upstream and downstream z vertex distribution. However, this isolation cut does not take into account the scattering and resolution effects of layer 1 hits. This is a source of a small number of events past Z_{cut} show in Figure 17 and will be improved in the future.

From Fig. 9, the cuts on the beam spot constrained vertex fit are useful for reducing downstream backgrounds although they are not enough to be used on their own without also requiring that the vertex projects back to the target position. In identifying downstream vertices, we use the unconstrained vertex collection to optimize our search for detached vertices. For each e^+e^- pair, we can see how the vertex changes when different additional constraints are applied. The unconstrained vertex collection only looks at the distance of closest approach between the two tracks. The target constrained vertex collection is optimized for a bump hunt analysis and requires that the vertex of the e^+e^- pairs occurs at the target. The beam spot constrained vertex collection requires that the momentum of the vertex pair projects back to the beam spot location at the target and considers the distance of closest approach between the two tracks. The beam spot constrained vertex fit quality, or vertex χ^2 , gives us information about how well the vertex momentum points

back to the beam spot location at the target. The beam spot constraint is useful in identifying events where a track has scattered significantly because the projected momentum misses the beam spot location at the target. Real signal events will always project back to the beam spot. While the beam spot constraint χ^2 includes information on the vertex projection to the target as well as the distance of closest approach of the two tracks at the vertex, studies of high z events show that downstream scatters produce events well beyond the xy vertex projection back to the target. The projection is shown in Fig. 12.

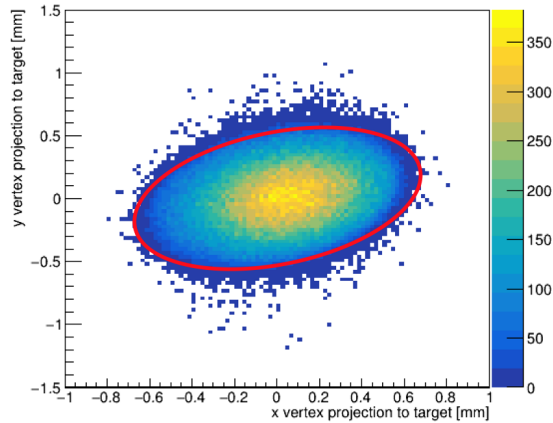


Figure 12: *The x and y momentum projection from the z vertex to the target is shown. We apply an elliptical, approximately 3σ cut to remove the periphery events resulting from scatters and vertexed pairs with mis-hits. This distribution shows the cut location after all other cuts have been applied.*

After selecting good quality reconstructed tracks and vertex using the SVT information only, the tracks are projected to their positions at the ECal and the quality of the matching of the track and ECal cluster is described as a multiple of the expected resolution function of the track momentum and position at the ECal. This parameter is a function of the number of deviations away from the mean in distributions from 2015 data. The matching parameter and relevant cut value are shown in Figure 13

The matching cut most significantly removes the small angle/low mass background events that we saw in Figure 9. The timing difference cut between the tracks and ECal clusters removes some out of time events, but the timing resolution on the clusters is more precise than the track time, and a cut on the two cluster time difference is critical for removing accidentals.

The two cluster time difference can be used to study the effects of cuts on accidentals as well as the contamination of accidentals in the final sample. The evenly spaced 2 ns peaks apparent in Figure 14 are due to accidental coincidences and the intrinsic 499 MHz electron beam bunch frequency. After all cuts are applied, the accidental contamination is less than 1% in the ± 2 ns event selection (this cut is the only one not shown in Figure 14). Separate studies using the accidental events to further identify sources of high z backgrounds showed that the contribution from accidentals was negligible.

We apply a cut to the momentum asymmetry designed to remove wide-angle bremsstrahlung (WAB) contributions to the data. In WAB backgrounds, an electron and photon are generated at the target, and the photon pair produces to an e^+e^- pair. Backgrounds arise when the initial scattered electron is vertexed with the pair-produced positron. In these events the electron typically carries much more energy than the counterpart photon in contrast to heavy photon generated e^+e^- pairs

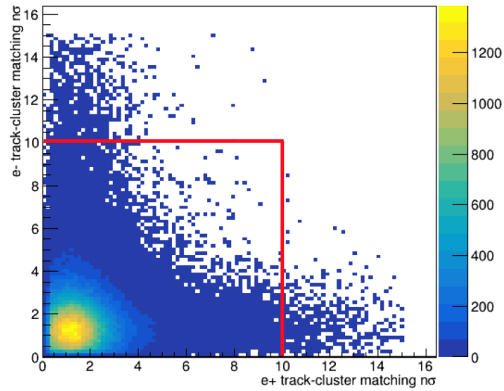


Figure 13: The track to cluster matching cut significantly improves our event selection. The parameterization is based on momentum and track projection to the calorimeter and was derived empirically from data. The cut is shown in red for both the e^- and e^+ .

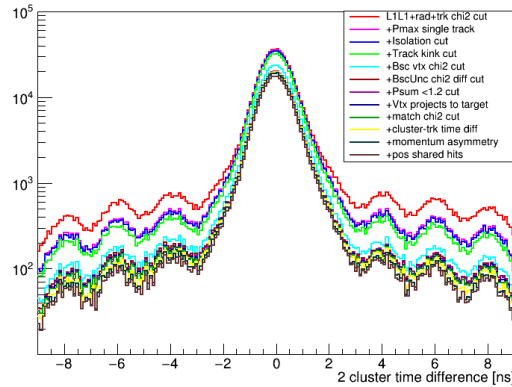


Figure 14: Cut effects on the two cluster time difference distribution for the L1L1 0.5 mm data set is shown on the left. The ratio of the two cluster time difference distribution in the final event selection (without the ± 2 ns cut) to those events in the initial event selection for the L1L1 0.5 mm data set is shown on the right.

which are somewhat symmetric in momentum.

Studies from high z background events in data showed that events where the positron track has 5 hits shared with another track in the event contribute significantly to down stream vertices. This is somewhat related to our isolation cut which does not account for hit position resolution effects and could still choose the wrong hit at layer 1. Further studies of the tracking ambiguities could potentially resolve these issues, but for now we eliminate these events to obtain a clean event sample. By removing tracks that only have a one hit difference with other tracks, the high z background in the data sample is reduced.

4 Setting limits on displaced A' 's

An upper limit on the heavy photon production at a given $m_{A'}$ and ϵ^2 is the maximum rate at which heavy photons could be produced, and still be consistent with the data. The confidence level used for this analysis is 90%: in other words, if a heavy photon signal does exist at a given rate, the limit set by this analysis will (incorrectly) exclude that signal rate only 10% of the time. The meaningful target for this analysis is the heavy photon production rate given by Equation (1). If the upper limit at a given $m_{A'}$ and ϵ^2 is below that rate, the analysis has (at 90% CL) excluded the possibility of a heavy photon at that $m_{A'}$ and ϵ^2 . Upper limits do not distinguish between a lack of sensitivity (insufficient data to say anything meaningful about the presence or absence of a signal) and the presence of a signal: the upper limit will be high in either case.

4.1. Treatment of high z backgrounds

According to the definition of the background model in Equation (4), we expect 0.5 background events per mass bin. Integrating over the mass range from 0.02–0.07 GeV would yield approximately 8 mass bins, and therefore, 4 events beyond the Z_{cut} . However, we see more events than this including vertices that don't appear consistent with this background fit as shown in Figure 15. To better estimate anticipated background we could expect beyond the Z_{cut} , we

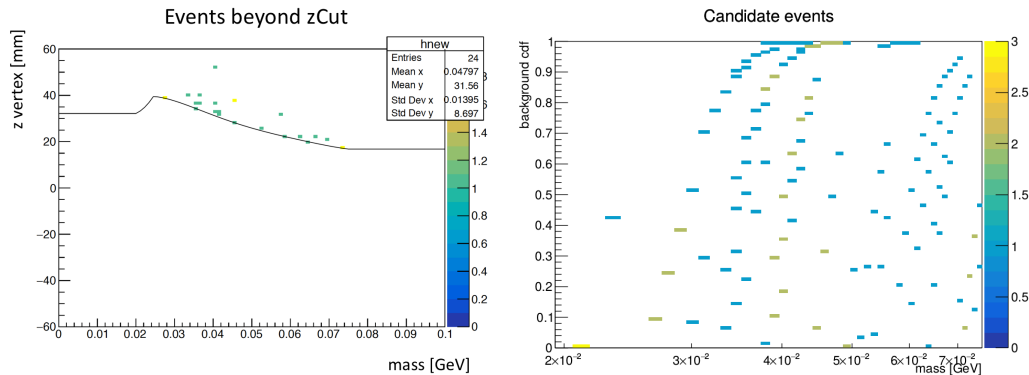


Figure 15: *Left: The unconstrained z vertex position for events in our data beyond the Z_{cut} (black line) are shown as a function of the invariant mass. Based on the background model, we expect around 0.5 events per mass bin. However, we see more events due to other backgrounds from sources such as double Coulomb scatters. Most events are close to Z_{cut} and some events are significantly beyond. Right: We characterize the high z events for each mass hypothesis (the same events can appear in several mass bins) by calculating the cumulative distribution function (CDF) using the background model and calculate their quantile for each mass hypothesis. Events close to unity show significant deviance from the background model while events close to 0 would be consistent with our background fit.*

generated a Monte Carlo sample that includes all simulated backgrounds in our experiment and has comparable statistics to our data. A comparison between both the data and Monte Carlo samples is shown in Fig. 16. In this Monte Carlo sample, we observed events beyond the Z_{cut} at rates that were statistically consistent with those observed in data. In re-calculating the average number of background events per mass bin, we calculate something closer to 2.6 background events (average) per mass bin (still higher than the observed 1.4 average background events per mass bin in Monte Carlo). Ongoing simulations attempt to fully characterize the background so we can improve our selection of events

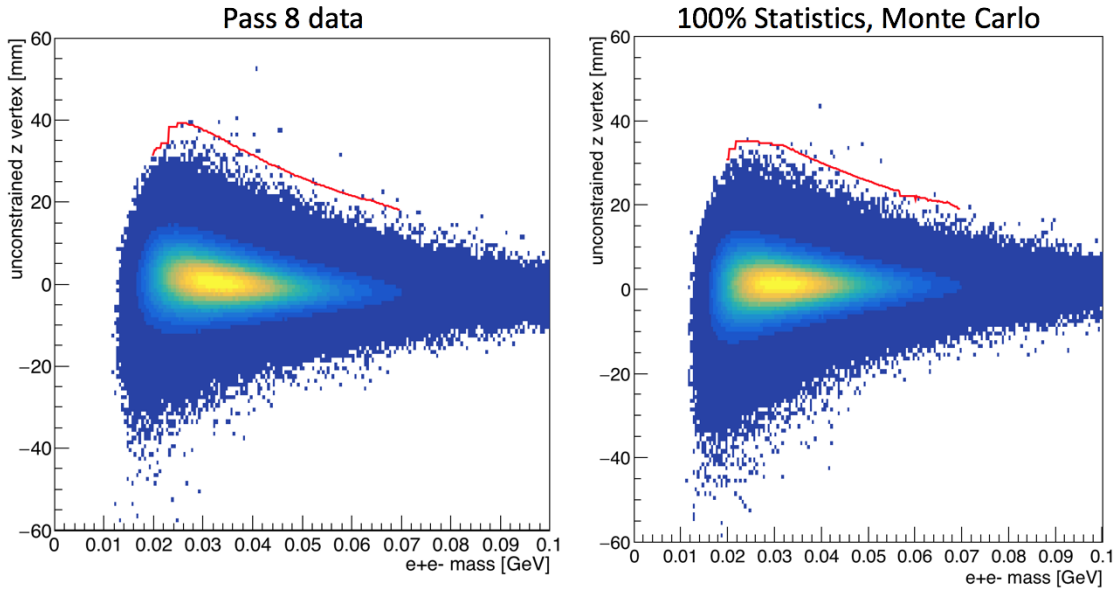


Figure 16: *Left: The z vertex versus mass distribution for our data is shown with the Z_{cut} (red). Right: The z vertex versus mass distribution for the 100% statistics Monte Carlo simulation of the backgrounds is shown.*

Further studies of these events in Monte Carlo shows evidence of double Coulomb scatters in layer 1 away from the beam that reconstruct a large downstream vertex. These events make up the majority of events past Z_{cut} . In the MC and the data, we also see evidence that a handful of the vertices beyond Z_{cut} are due to one track picking up the wrong hit in layer 1 (the incorrect hit is closer to the beam) coupled with a large scatter away from the beam. In principle, the isolation cut should remove these events. However, the current isolation cut does not account for resolution effects due to multiple scattering. The MC shows that such events have a large layer 1 scatter towards the beam which causes the track to pick up the wrong event and still pass the isolation cut. Both of these processes are shown schematically in Figure 17.

4.2. Optimum Interval Method

The method chosen for setting limits is the “optimum interval” method by Yellin [S. Yellin, 2002]. This method was developed for dark matter direct detection experiments, and is intended for experiments where the signal shape is known, but the backgrounds are not fully understood and there is the possibility of an unexpected background. A particular strength of the method is that it minimizes the influence of a background that is concentrated in one part of the data distribution. This analysis uses Yellin’s implementation of the optimum interval method, which is publicly available [S. Yellin, 2011].

The optimum interval method sets a one-sided upper limit (with confidence level C) on the number of signal events μ in a one-dimensional data set, where the shape of the signal distribution is known. For HPS, the data set is the distribution of vertex z locations, after applying the mass and z_{cut} cuts; the signal distribution is the $s(z)$ found in Section 2 for the $m_{A'}$ and ϵ^2 being tested.

The method works by testing a proposed signal rate μ against the data with a confidence level C . The cumulative distribution function of the signal, $S(z)$, is known. A change of variables is made from the measured variable z to a new variable $x = \mu S(z)$. Under the signal assumption,

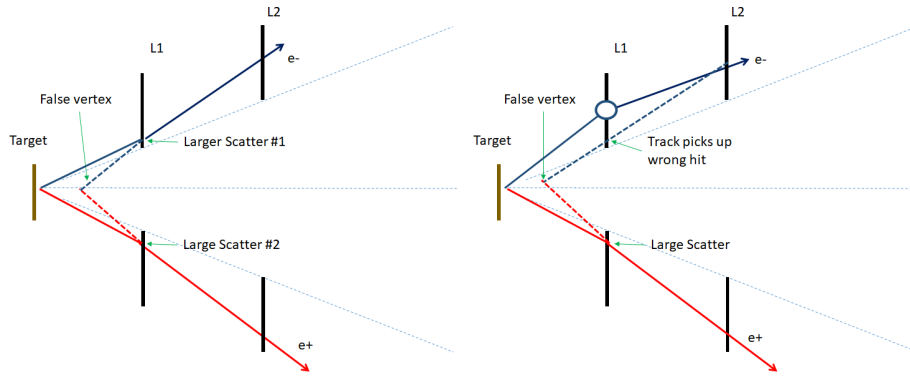


Figure 17: Left: Schematic of large z backgrounds due to double large scatters away from the beam. These large scatters could be due to multiple scattering, a single large Coulomb scatter, or a combination of both. These types of events make up most of the events past Z_{cut} according to MC. Right: Schematic of large z backgrounds due to a single large scatter (either from multiple scattering or Coulomb scattering) in coincidence with picking up the wrong hit in layer 1. Because the incorrect hit is closer to the beam, the vertex is downstream from the target.

the expected distribution of the data is uniform in x with unit density, and has total width μ . An interval (x_1, x_2) , with $x_1, x_2 \in [0, \mu]$, contains a number of expected signal events equal to its width $\Delta x = x_2 - x_1$. If an unexpected background is present and is distributed differently from the signal, the data will not be distributed uniformly in x , and events will be spaced more widely where the background is not present.

The next step is to search for the “optimum interval,” the interval that most strongly rejects the proposed signal rate. This is the interval (x_1, x_2) that contains the smallest number of actual events n relative to its width Δx . Put another way, if the function $C_n(\Delta x, \mu)$ is the probability that all intervals of width Δx contain more than n events, the optimum interval is the (x_1, x_2) that maximizes $C_n(\Delta x, \mu)$.

For the optimum interval, x_1 and x_2 always coincide with 0, μ , or events in the data (otherwise the interval can be widened to increase Δx without changing n). Thus the program only needs to loop over every interval between two events, of width x expected events and containing n actual events. The value of $C_n(\Delta x, \mu)$ for the optimum interval is called C_{Max} , and if it exceeds a threshold $\bar{C}_{Max}(C, \mu)$, μ is rejected with confidence level C . The upper limit on μ is the value for which $C_{Max} = \bar{C}_{Max}(C, \mu)$.

The function $C_n(x, \mu)$ is the probability that all intervals containing n events are narrower than this one (that is, that no interval with n events has this low a ratio of actual to expected events). The interval with largest value of $C_n(x, \mu)$ is the “optimum interval” that most strongly rejects the proposed signal rate. The largest value found is called C_{Max} , and if it exceeds a threshold $\bar{C}_{Max}(C, \mu)$, μ is rejected with confidence level C . The upper limit on μ is the value for which $C_{Max} = \bar{C}_{Max}(C, \mu)$.

The functions $C_n(x, \mu)$ and $\bar{C}_{Max}(C, \mu)$ pay the statistical penalties for using the data to pick the best interval. Since they are not specific to the signal distribution, they are calculated using Monte Carlo and stored in lookup tables that are distributed with the software.

Here we use the optimum interval method to set a limit as we do not precisely know the shape of our background model. The optimum interval method can be used with a known background; in this case, the known background density is added to the signal density. Since the expected background for HPS falls off rapidly, relatively little is to be gained from this: after the cut in z , the

remaining known background is tightly clustered at the edge of the range of z , so the optimum interval method effectively ignores it even without subtraction. Therefore the known background is not used as an input to the optimum interval calculation.

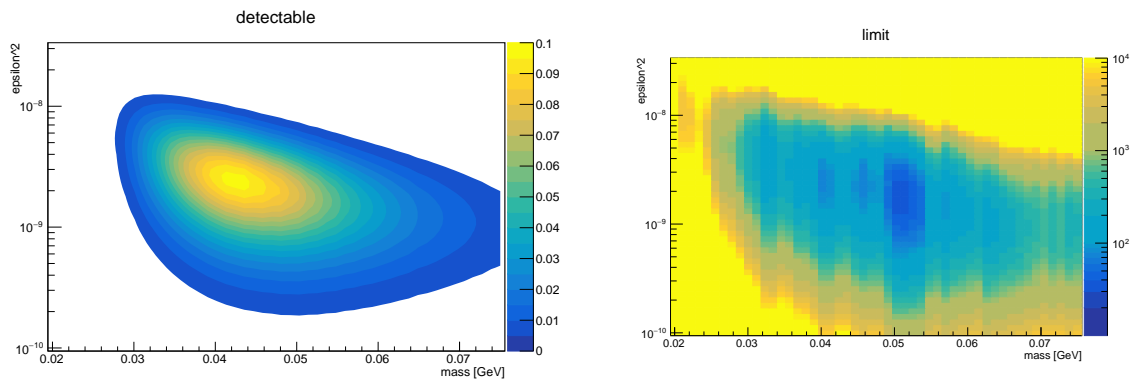


Figure 18: Left: The number of A' s we expect to detect with a maximum of 0.097 events is shown where A' production is maximal at a mass of 43.6 MeV and ϵ^2 coupling of $2.4E - 9$. Right: 90% CL upper limit on μ/μ_{exp} , the ratio of the true production rate to the expected production rate for a heavy photon. A value of 1 would mean exclusion; the lowest contour on this plot is 35.7 at a mass of 51.4 MeV and coupling of $1.7E - 9$. The vertical ridges in this plot correspond to the locations of events in mass space.

5 Systematics

Systematics for the displaced vertex search are currently in progress. However, an estimate is shown in Table 3. The sources of identified systematics are the radiative fraction, the target position, and the mass resolution from Møllers. The target position affects both the mass resolution and the A' efficiency due to differences in acceptance. The radiative fraction and mass resolution systematics are well understood from the bump hunt analysis [O. Moreno, 2017], and we don't expect them to differ significantly for the vertex analysis. However, the target position is in a different place than the bump hunt (farther than it's "true" value), so we expect the systematic to be larger.

Table 3: *Systematics*

Systematic Error	Value
Radiative Fraction	$\sim 7\%$
Target Position	$\sim 2\%$
Mass Resolution	$\sim 3\%$

6 Conclusion

A search for displaced heavy photons in the mass range between 20–70 MeV and decaying to e^+e^- pairs was performed using the 2015 HPS engineering run. This analysis focused on events with tracks in the first layer of the SVT while the SVT was at the nominal ± 0.5 mm above and below the beam line. The backgrounds and cuts were initially tuned on a 10% blinded sample and later optimized using the full data set. The analysis was conducted on the full data set as it was necessary to fully understand the backgrounds downstream of the target and the acceptance related inefficiencies that were not fully accounted for in the proposal reach estimates. In addition to unblinding the data, we were able to compare the high z backgrounds to those seen in a comparable Monte Carlo sample, generated with full backgrounds and statistics. Despite some additional background remaining even after optimization of event selection, we used the optimum interval method to establish our procedure for limit setting even in the event of some additional or unknown background. No significant signal was observed in our data, but no formal limit could be set using only the 1.7 days of running. With further improvements to our trigger and an additional tracking layer between the target and the first layer of the SVT, we anticipate recovery of our reach and anticipate using the procedures and practices studied here to establish limits in future running.

References

- [P. Billoir, 1992] P. Billoir and S. Qian (1992). Fast Vertex Fitting with a Local Parametrization of Tracks NIM Volume 311; Issues 1-2
- [S. Yellin, 2002] S. Yellin (2002). Finding an Upper Limit in the Presence of Unknown Background. arXiv:physics/0203002
- [S. Yellin, 2011] S. Yellin (2011). Some Ways of Combining Optimum Interval Upper Limits. arXiv:1105.2928
- [O. Moreno, 2017] O. Moreno, N. Baltzell, M. Graham, and J. Jaros (2017). Search for a Heavy Photon in Electro-Produced e^+e^- Pairs with the HPS Experiment at JLab. Analysis Note
- [S. Uemera, 2016] S. Uemera (2016). Searching for Heavy Photons in the HPS Experiment. PhD Thesis
- [H. Szumila-Vance, 2017] H. Szumila-Vance (2017). Search for Heavy Photons with Detached Vertices in the Heavy Photon Search Experiment. PhD Thesis